Journal of Environmental Health Science and Engineering (2022) 20:617–628
https://doi.org/10.1007/s40201-021-00762-2

RESEARCH ARTICLE

Photocatalytic degradation of bisphenol a from aqueous solution using bismuth ferric magnetic nanoparticle: synthesis, characterization and response surface methodology-central composite design modeling

Mohammad Hassan Mahmoudian[1] · Alireza Mesdaghinia[2,3] · Amir Hossein Mahvi[2] · Simin Nasseri[2,3] · Ramin Nabizadeh[2] · Mohammad Hadi Dehghani[2]

Received: 3 July 2021 / Accepted: 23 November 2021 / Published online: 24 June 2022

Abstract

Purpose Bisphenol A (BPA), as endocrine-disrupting compound (EDC), is extensively used as an important chemical in the synthesis of polycarbonate polymers and epoxy resins. BPA absorption into the body can result in the development of metabolic disorders such as low sex-specific neurodevelopment, immune toxicity, neurotoxicity and interference of cellular pathway. Therefore, the presence of BPA in the body and the environment can create hazards that must reach standards before being discharged into the environment.

Methods In this study, bismuth ferric nanomagnetic (BFO NMPs) were successfully synthesized via sol-gel method and developed as photocatalysts for BPA removal under visible light irradiation. FE-SEM, TEM, PL, XRD, UV-Vis DRS, VSM, EDX, and FTIR were used to characterize the BFO NMPs.

Results RSM model ($R^2 = 0.9745$) showed a good correlation between experimental and predicted removal efficiency of BPA. The investigation of four independent variables indicated that pH had the most significant positive effect on the degradation of BPA. Under optimal conditions (pH = 4.042, catalyst dose = 7.617 mg, contact time = 122.742 min and BPA concentration = 15.065 mg/L), maximum degradation was calculated to be 98.7%. After five recycles, the removal of BPA remained >82%, which indicated the proper ability to reuse the catalyst.

Conclusion In conclusion, it can be stated like BPA, the prepared BFO NMPs is a promising photocatalyst for practical application in organic pollutant decomposition.

Keywords Bisphenol a · BFO MNPs · Photocatalytic degradation · Response surface method

Introduction

Phenol is formed by a hydroxyl group attached to benzene ring. Bisphenol A (BPA), by a condensation reaction synthesized, in acidic condition from phenol and acetone [1–5]. BPA, an endocrine-disrupting compound (EDC), is extensively used as an important chemical in the synthesis of polycarbonate polymers and epoxy resins [6, 7]. A variety of chemicals with structural or functional similarity to BPA have been identified in foodstuffs [8]. Corpuscular function could disrupt even at very low concentration (0.23 ng/l) of BPA, leading to a wide spectrum of harmful health effects. However, BPA is able to easily leak into the human body [9]. A study found that 92% of participants were detected BPA in their urine [10] and less values in

✉ Alireza Mesdaghinia
mesdaghinia@tums.ac.ir

1 Department of Environmental Health Engineering, School of Public Health, International Campus, Tehran University of Medical Sciences (IC–TUMS), Tehran, Iran

2 Department of Environmental Health Engineering, School of Public Health, Tehran University of Medical Sciences, Tehran, Iran

3 Center for Water Quality Research, Institute for Environmental Research, Tehran University of Medical Sciences, Tehran, Iran

human biological specimens [11]. However, it is expected there is a poor understanding of the potential toxicity of the most BPA analogues. Some studies showed an association between BPA analogues and fasting blood glucose, diabetes, or insulin resistance [11, 12]. These compounds result in reproductive and sexual abnormalities such as hormone-dependent cancers, sperm counts decline in males and reduction in reproductive fitness [6, 13, 14]. Annually, three million tons of BPA are produced in the world. It is frequently found in all of environmental matrix including air, water and soil because of the massive amount of its utilization and high persistency [14]. Fortunately, due to the small bioconcentration factor and octanol-water partition coefficient, BPA has a small potential for bioaccumulation. However, BPA seems to be biodegradable only by a small number of microorganisms [15]. Consequently, leaching processes which are decomposed BPA derived from various industrial can reach surface and groundwater and contaminate them [9]. However, BPA is slightly soluble in water (120–300 mg/l at 25 °C) and is usually released in the discharge from construction units using BPA based products. The half-life of BPA in surface and ground water is estimated to be 1–150 and 2–360 days, respectively [15]. BPA does not exist freely in nature and undergoes photo-oxidation with a half-life about 0.2 days in air [15]. Therefore, there is an increasing interest to find adequate and affordable technologies for removal and degradation of BPA from water body [16]. Existing conventional wastewater treatment plants (WWTPs) are not able to treat effectively persistent compounds such as BPA [6, 17, 18]. Thus, many researchers have conducted studies on the development of effective and sustainable treatment methods in order to set a barrier to the release of emerging contaminants such as BPA into the environment [17, 19–22].

Nowadays photocatalysis-based methods are a promising technology due to their high efficiency, complete pollutants mineralization to CO_2, simplicity of operation and low cost [23]. In photocatalytic oxidation processes, an electron is rejected from the valence band (VB) to the conduction band (CB) of the semiconductor under UV or visible radiation and produces highly reactive spices mainly hydroxyl radicals (OH^*) which are then attack the organic pollutants and are eventually mineralized into CO_2 and inorganic anions [6, 13, 16]. To date, photocatalysts such as TiO_2, SnO_2, and ZnO have been extensively used as efficient materials for solving environmental and energy problems because of their efficient photocatalytic degradation, high chemical stability, and non-toxicity [24–27]. However, among the main drawbacks are their large bang gap which absorb only 5% sunlight in the ultraviolet region and rapid recombination of electron-hole pairs [14, 23, 27, 28]. BPA is not sensitive to hydrolysis but if not bound to organic matters, it has a potential to photolysis in water [15]. As a result, it is very essential to synthesis and develops new photocatalyst materials with strong absorbance in visible light region. Currently, by optimizing the conditions and using semiconductors in photocatalytic processes, conversion of organic compounds to water and carbon dioxide has become possible.

Recently, a new photocatalyst, perovskite bismuth ferric (BFO) exhibited high photocatalytic activities under visible light irradiation for water splitting and degradation of organics because of its narrow band gap, excellent chemical stability, ferroelectric, and ferromagnetic properties [27–30]. In addition, optimization of influential variables using statistical experimental design mainly Response Surface Method (RSM) has received plentiful attention in environmental applications because of predicting combined effects of independent variables on response at the time and lower number of experiments [23, 31–33]. The present study will examine model and optimize the removal of BPA with a BFO catalyst synthesized by sol-gel method. So far, very few studies have examined this issue, and almost no study has examined the modeling and optimization BPA removal conditions with this catalyst. It is hoped that the current study will yield very good results in the system under study condition. As such, in this study, BFO NMPs photocatalyst with a particle diameter less than 100 nm is synthesized by sol-gel method and its photocatalytic activity will be investigated in the degradation of BPA under visible light irradiation. The studied variables include pH, photocatalyst concentration, BPA initial concentration, and reaction time. Four-factor Central Composite Design (CCD) based with Response Surface Method (RSM) would be used to optimize the response as photodegradation percentage of BPA using BFO NMPs.

Materials and methods

Chemicals

All the chemical and reagents were of analytical grade and used in the current study without any further purification. Bismuth nitrate (($Bi(NO_3)_3.5H_2O$), ≥98%), iron nitrate (($Fe(NO_3)_3.9H_2O$), >98%), acetic acid (glacial ≥99%), and Hydrochloric acid (HCl, 35–37%) were provided by Sigma Aldrich company (St. Louis, MO, USA). Sulfuric acid (H_2SO_4, 98%) and bisphenol A were prepared by Merck Company (Darmstadt, Germany). Double distillated water was used for preparation of all samples (18.2 MΩ cm).

Preparation of BFO NMPs

Firstly, 0.016 mol of Bi $(NO_3)_3.5H_2O$ was dispersed in ethylene glycol in an ultrasonic bath. To form a clear, homogenous solution was sonicated for 2 min at a temperature of 25 °C. In order to obtain a brownish red sol, a stoichiometric amount of Fe $(NO_3)_3.9H_2O$ was added to above solution and

sonicated for another 10 min at the same temperature. After that, the prepared solution was kept in the oven at a temperature of 60 °C for 24 h to form a xerogel. Eventually, xerogel powder was calcinated at 500 °C for 0.5 h at a heating rate of 6 °C/min to obtain BFO NMPs [34].

BFO NMPs characterization

Crystalline structure of BFO NMPs was studied using X-Ray Diffractometer (XRD. Rigaku, step size 0.02°, scan speed 4°/min) with Cu-Kα as source radiation at a wavelength 0.154 nm. The Transmission Electron Microscope (TEM) PHILIPS, CM30 Netherlands, V = 200KV. The Fourier transform infrared spectra (FTIR) was taken using KBr as a reference material within the range of 400–4000 cm^{-1} with a resolution of 4 cm^{-1} and 16 scans (Beijing, Rayleigh WQF-510A). The surface morphology of prepared BFO NMPs samples was surveyed by field emission scanning electron microscopy (FE-SEM, FEI Nova NanoSEM® 450; EDX, Bruker Xflash® 6 | 10). AvaSpec spectrophotometer (Avantes AvaSpec 2048 TEC) was used to measure UV–vis diffuse reflectance spectra (DRS) by using $BaSO_4$ as a reference material. Photoluminescence (PL) spectra of BFO NMPs samples were recorded on Agilent G9800A Cary Eclipse Fluorescence Spectrophotometer. Magnetic properties of the BFO NMPs were determined using vibrating specimen magnetometer (VSM, Varian, V-7300 Series 12).

Photocatalysis process

BPA was selected to assess the photocatalytic activity of BFO NMPs under visible light radiation. All examinations were conducted at room pressure and temperature (25 ± 1 °C). Photochemical test was performed in 50 mL Erlenmeyer flask using a 25 W white LED lamp (contains five LED lamps) as visible light source. Photocatalytic experiments were done in 25 mL solutions with predetermined independent parameters under magnetic stirrer at a speed of 350 rpm. The suspension of BFO NMPs was kept in dark for half an hour to reach adsorption-desorption equilibrium before light illumination for each experiment. At the end of each experiment, suspension was centrifuged at a speed of 8000 rpm for 10 min. Initial and residual concentration of BPA at supernatant was measured by spectrophotometer at wavelength of 277 nm. Removal efficiency of BPA was calculated with Eq. (1) [27, 35]:

$$\text{Removal efficiency } (\%) = \frac{(C_0 - C)}{C_0} \times 100 \quad (1)$$

where C_0 and C are initial and final concentration of the BPA solution, respectively.

Experimental design

Optimization of the process variables and their interactions in this study was performed using RSM. RSM is a particular set of mathematical and statistical methods that are used to design experiments, build models, evaluate the effects of variables, determine the optimum amount of variables for predicting targeted responses, improve the performance of parameters, and decrease the inaccuracy of experiments [31, 32]. CCD is the most commonly used class of second-order designs under RSM [23, 36]. Such a design has been abundantly applied for removal of many pollutants with photocatalysis process [37–42]. For *n* independent variables, the number of experiments in CCD was predicted using following equation:

$$N = 2^n + 2n + n_C \quad (2)$$

Where, 2^n, $2n$ and n_c are factorial runs, axial runs and center runs, respectively. In the present study, $N = 2^4 + 2 \times 4 + 6 = 30$. A five level CCD and range of independent variables suggested by Design Expert V11.1.1.0 software (Stat Soft Inc., Tulsa, USA) are shown in Table 1. A quadratic equation model was used to optimize the process variables as follow:

$$y = b_0 + \sum_{i=1}^{4} b_i X_i + \sum_{i=1}^{4} \sum_{i=1}^{4} b_{ij} X_i X_j + \sum_{i=1}^{4} b_{ii} X_i^2 \quad (3)$$

Where, y is the response variable (BPA removal, %), x_i and x_j are the independent variables (initial BPA concentration, solution pH, adsorbent dose, and reaction time) known for each run, b_0 is the model constant; b_i is the linear coefficient, b_{ii} is the quadratic coefficient, and b_{ij} is the interaction coefficient. The value of alpha coefficient was selected to be 2.

Table 1 level of the independent variables in CCD for removal of BPA

Coded variables (X_i)	Variables	unit	Experimental range				
			-α	−1	0	+1	+α
X1	Contact time	min	5	35	65	95	125
X2	pH	–	3	5	7	9	11
X3	Catalyst dosage	g/100 ml	5	20	35	50	65
X4	BPA concentration	mg/L	5	10	15	20	25

Results and discussion

BFO NMPs characteristics

The FE-SEM Fig. 1(a and b) revealed that BFO NMPs has smooth, regularly spherical crystals and particle size of BFO NMPs which is relatively uniform [43, 44]. TEM micrographs (fig. 1c and d) of BFO are shown in zoom in as 500 nm and 50 nm. These Nano magnetic particles consist of nearly round shape particles ranging from 50 to 100 nm, which is consistent with the FESEM of perovskite-phase BFO and XRD calculations, as shown in fig. 1a and b. According to Fig. 1b, it can be seen that the magnetism of the particles has caused the small particles to stick together and agglomerate. Photoluminescence spectra were employed to investigate the recombination rate of photoinduced electrons and holes pair as shown in Fig. 1(e). BFO NMPs sample has intensive peak at 469 nm, which indicates the high rate of electron-hole recombination leading to low photocatalytic activity [23, 27]. Figure 1(d) shows the XRD patterns of BFO NMPs samples. The diffraction peaks at 2Θ values of 22.4°(101), 31.08°(110), 37.8°(004), 39.49°(202), 45.79°(200), 51.58°(105) and 56.98°(211), clearly showed the phase of BFO NMPs [43]. Sharp and strong peaks implied that the BFO NMPs sample has high crystallinity [23]. The presence of peak-splitting in XRD pattern reveals rhombohedral, consistent and ceramic structure of BFO NMPs [44, 45]. The Scherer equation used to calculate the average of crystalline size (Eq. (4)).

$$\tau \frac{K\lambda}{\beta cos\theta} = \tag{4}$$

Where, τ is the medium size of crystallite as nm, K is the crystalline shape coefficient (between 0.62 to 2.08), λ is the X-ray tube Wavelength, β is the FWHM, and θ is the X-ray diffraction angle. It should be mentioned that particle sizes calculated by XRD analyses are commonly smaller than those found by TEM.

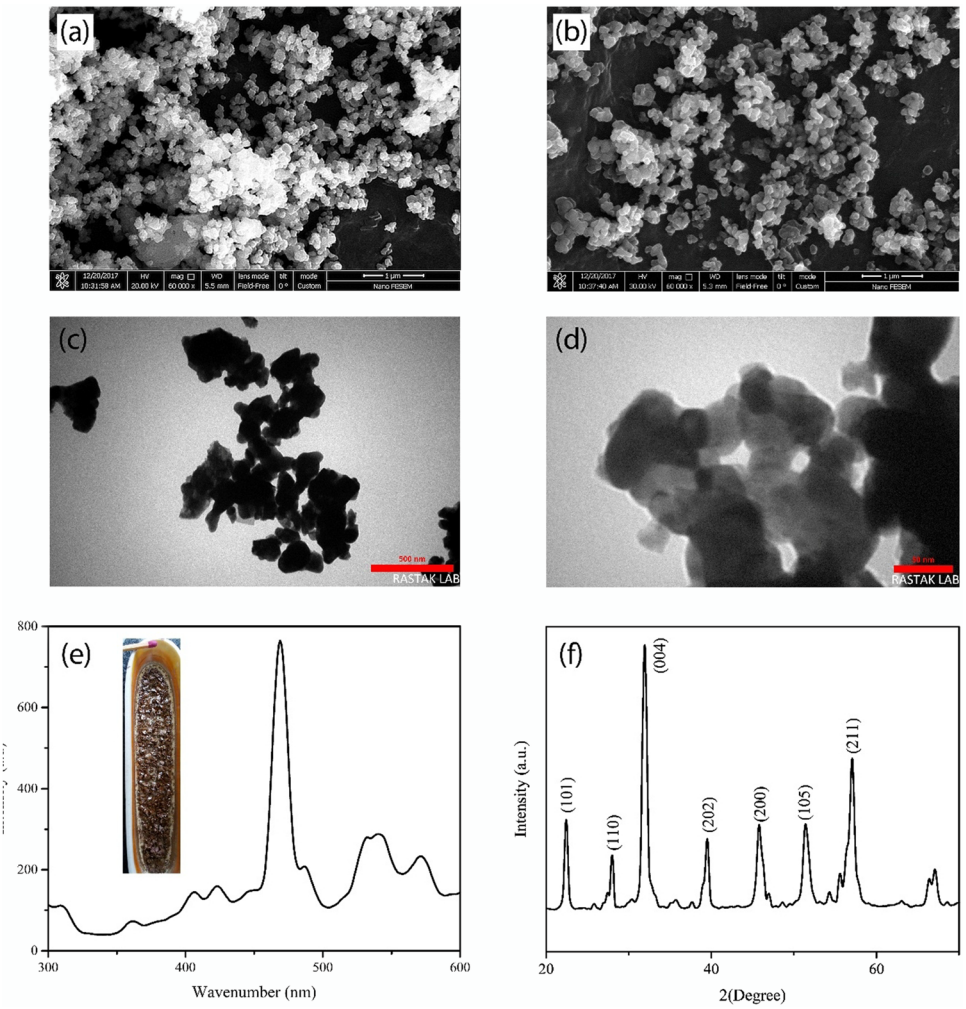

Fig. 1 **a** and **b** FESEM image in two different type, **c** TEM in 500 nm and **d** TEM in 50 nm scaling **e** PL curve, **f** XRD pattern of BFO NMPs.

UV–Vis Diffuse Reflectance Spectrum (UV-Vis DRS) of synthesized BFO NMPs is shown in Fig. 2(a). It can be seen that BFO NMPs absorb light in the range of 300–800 nm. Absorption edge of BFO NMPs was obtained by drawing a tangent line on the adsorption curve [23, 46] and found to be 600 nm, implying that the BFO NMPs material can absorb visible light in the wavelength range of 400–600 nm. The energy band gap of indirect semiconductor can be calculated by Eq. (5) [43, 47]:

$$E_g = \frac{1239.8}{\lambda} \quad (5)$$

where E_g(eV) is the band gap and, λ is the wavelength of optical adsorption edge (nm). As a result, the energy band gap of BFO NMPs sample was found to be 2.07 eV. In this study, the band-gap energy of BFO NMPs was smaller than those reported by other authors [44, 46, 48, 49].

VSM analysis was performed for BFO NMPs at room temperature using a vibrating magnetometer (Fig. 2(b)). This analysis was carried out on a magnetic field of ±10 H (KG) and in a saturation magnetization range of ±10 emu/g. The results showed that the maximum saturation magnetization for the BFO NMPs was equal to 5.8 emu/g. These results clearly demonstrated the appropriate magnetic property of the synthesized BFO NMPs. Figure 2(c) shows the Energy-dispersive X-ray spectroscopy of BFO NMPs. The major elements in BFO NMPs sample were Bi, Fe and O with the weight percentage of 61, 21.66 and 12.35 eV, respectively.

Figure 2(d) shows the FTIR spectra of BFO MNPs. As is shown here, seven peaks appeared for BFO NMPs of which five peaks are weak, one of them is sharp and another one is wide peak, which are assigned to the Fe-O, Bi-O and O-H stretching vibration mode. Therefore, IR peaks less than 1000 cm^{-1} such as 815, 560 and 439 are related to the vibrations bands of Fe-O and Bi-O, respectively.

Modeling and statistical analysis

The designed experiments suggested by CCD were performed as shown in Table 2. Then, the results of each experiment as response were entered into the software and analyzed using analysis of variance (ANOVA). A quadratic model was developed to predict response values (BPA removal) as Eq. (6):

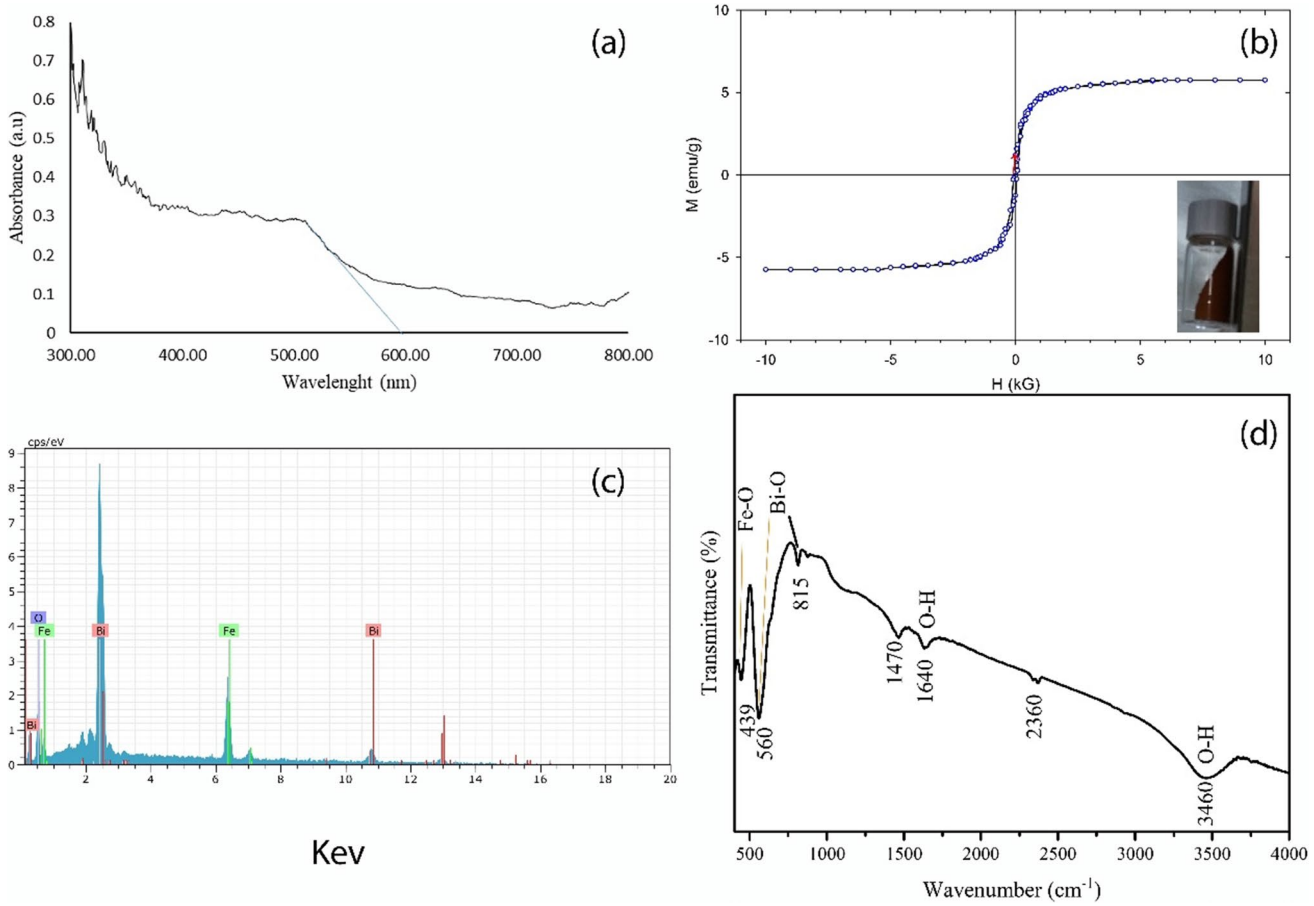

Fig. 2 **a** UV-visible DRS, **b** VSM analysis, **c** EDX analysis, **d** FTIR analysis of BFO NMPs sample

Table 2 The experimental runs designated by CCD

Std	Run	Factor 1 X1: Time	Factor 2 X2: pH	Factor 3 X3: BSA Con.	Factor 4 X4: Cat. Dose	Response 1 BSA Removal
		min	–	mg/L	mg/100 mL	%
13	1	35	5	50	20	54
8	2	95	9	50	10	25
28	3	65	7	35	15	42
2	4	95	5	20	10	75
20	5	65	11	35	15	6
24	6	65	7	35	25	51
26	7	65	7	35	15	32
5	8	35	5	50	10	43
15	9	35	9	50	20	25
14	10	95	5	50	20	54
19	11	65	3	35	15	70
4	12	95	9	20	10	23
22	13	65	7	65	15	46
10	14	95	5	20	20	83
6	15	95	5	50	10	56
25	16	65	7	35	15	37
9	17	35	5	20	20	71
17	18	5	7	35	15	42
23	19	65	7	35	5	40
27	20	65	7	35	15	35
1	21	35	5	20	10	68
3	22	35	9	20	10	11
21	23	65	7	5	15	56
12	24	95	9	20	20	43
7	25	35	9	50	10	16
16	26	95	9	50	20	43
11	27	35	9	20	20	26
29	28	65	7	35	15	31
18	29	125	7	35	15	60
30	30	65	7	35	15	36

$$y = 35.5 + 5.17X_1 - 17.17X_2 - 4.33X_3 + 4.33X_4 + 1.5X_1X_2 - 0.5X_1X_3 + 0.38X_1X_4 + 6X_2X_3 + 2.63X_2X_4 - 0.62X_3X_4 + 3.52{X_1}^2 + 0.77{X_2}^2 + 3.52{X_3}^2 + 2.15{X_4}^2 \quad (6)$$

The results of ANOVA for BPA removal at significance level < 0.05 are shown in Table 3. Besidep value, coefficient of determination (R^2) and lack of fit were selected to judge on ability of the model to predict response values [23, 32, 50, 51]. According to ANOVA results, the linear effect of terms X_1, X_2, X_3, X_4, the interaction effect of terms X_2X_3 and X_2X_4, and quadratic effect of terms ${X_1}^2$, ${X_3}^2$ and ${X_4}^2$ were found to be significant. Among process variables, pH (X_2) and contact time (X_1) had the most negative and positive effect on response variable, respectively. This means that when pH variable increases, PBA removal decreases and with the increase of contact time, BPA removal increases as well. The R^2 value of 0.9745 and p value<0.0001 show that the second-order regression model obtained for BPA photocatalytic degradation using BFO NMPs is well-satisfied. The predicted R^2 of 0.88 is in reasonable agreement with the adjusted R^2 0.95 (the difference is less than 0.2).

Effect of independent variables on photocatalytic degradation of BFO NMPs

Figure 3(a) shows the combined effect of contact time and BPA concentration at constant values of pH = 7 and catalyst dosage = 15 g/100 L. It can be seen that with increasing contact time from 35 to 95 min, removal efficiency increased from 34 to 52.7%. Figure 3(b) suggests that removal efficiency decreases with increasing BPA concentration from 20 to 50 mg/L. This can be related to decreasing the number of available reactive sites and saturation of them on BFO NMPs as well as decreasing

Table 3 The results of ANOVA for percentage of BFO NMPs removal

Source	Sum of Squares	df	Mean Square	F-value	p value	
Model	10,314.33	14	736.74	40.88	< 0.0001	significant
Time	640.67	1	640.67	35.55	< 0.0001	significant
pH	7350.00	1	7350.00	407.83	< 0.0001	significant
BPA concentration	450.67	1	450.67	25.01	0.0002	significant
Catalyst Dosage	450.67	1	450.67	25.01	0.0002	significant
Time*pH	36.00	1	36.00	2.00	0.1780	not significant
Time*BPA concentration	4.00	1	4.00	0.2219	0.6443	not significant
Time*Catalyst Dosage	2.25	1	2.25	0.1248	0.7288	not significant
pH*BPA concentration	576.00	1	576.00	31.96	< 0.0001	significant
pH*Catalyst Dosage	110.25	1	110.25	6.12	0.0258	significant
BPA concentration*Catalyst Dosage	6.25	1	6.25	0.3468	0.5647	not significant
Time ^{2}	356.30	1	356.30	19.77	0.0005	significant
pH ^{2}	3.44	1	3.44	0.1909	0.6684	not significant
Catalyst Dosage ^{2}	356.30	1	356.30	19.77	0.0005	significant
BPA concentration ^{2}	136.30	1	136.30	7.56	0.0149	significant
Residual	270.33	15	18.02			
Lack of Fit	192.83	10	19.28	1.24	0.4281	not significant
Pure Error	77.50	5	15.50			
Cor Total	10,584.67	29				
User Std. Dev.	4.245			R^2	0.974	
Std. Dev.	4.24			Adjusted R^2	0.95	
Mean	43.33			Predicted R^2	0.88	
C.V. %	9.79			Adeq Precision	26.011	

path length of the photons entering the solution [52, 53]. Solution pH is one of the main influential parameters in adsorption and photocatalytic processes because of protonation/deprotonation of pollutants and catalyst surface [23, 28, 52, 53]. According to Fig.3(c), maximum removal of BPA was observed at lower pH of solution based on previous studies [54] . With increasing pH from 5 to 9, removal percentage decreased from 53 to 12%. At low pH, positive holes are responsible as the major oxidation species, whereas in neutral or high pH, hydroxyl radicals are the predominant species [28]. Furthermore, under basic conditions, the BFO MNPs surface becomes negatively charged that leads to a repulsing of the negatively charged BPA molecules. In the present study, the throughout degradation rate increased with decreasing pH with optimum at pH = 5. The photocatalyst dosage is another important parameter in photocatalytic degradation of organic pollutants [28, 52]. In this study, photocatalyst dosage was found to be in the range of 5 to 25 g/100 mL. As expected, at constant values of initial BPA concentration 35 mg/L and contact time 65 min, an increase was observed in removal efficiency of BPA with increasing photocatalyst dosage from 10 to 20 g/100 L. This originated from higher number of active sites on the photocatalyst and consequently increased the absorption of the number of BPA molecules and photons [23, 28, 52, 53]. Almost all catalysts are able to provide sites for generating free radicals that promote the reaction.

Process optimization and model validity

To optimize the BPA removal, all the parameters were evaluated in the range as shown in Table 2, while the response (degradation percentage) was selected at the maximum value. The outcome of the model indicates that the maximum efficiency (100%) is obtained at pH = 4.042, catalyst dose = 7.617 g/100 mL, contact time = 122.742 min and BPA concentration = 15.065 mg/L. In order to validate the accuracy of the optimization model, a study on photocatalytic degradation of BPA was conducted in the batch reactor under optimum conditions. The experimental value of photocatalytic degradation test was found to be 98.7%, which is very close to the predicted value (100%). Hence, the optimum conditions suggested by RSM are valid and RSM is a good tool to optimize photocatalytic degradation process of BPA using BFO NMPs.

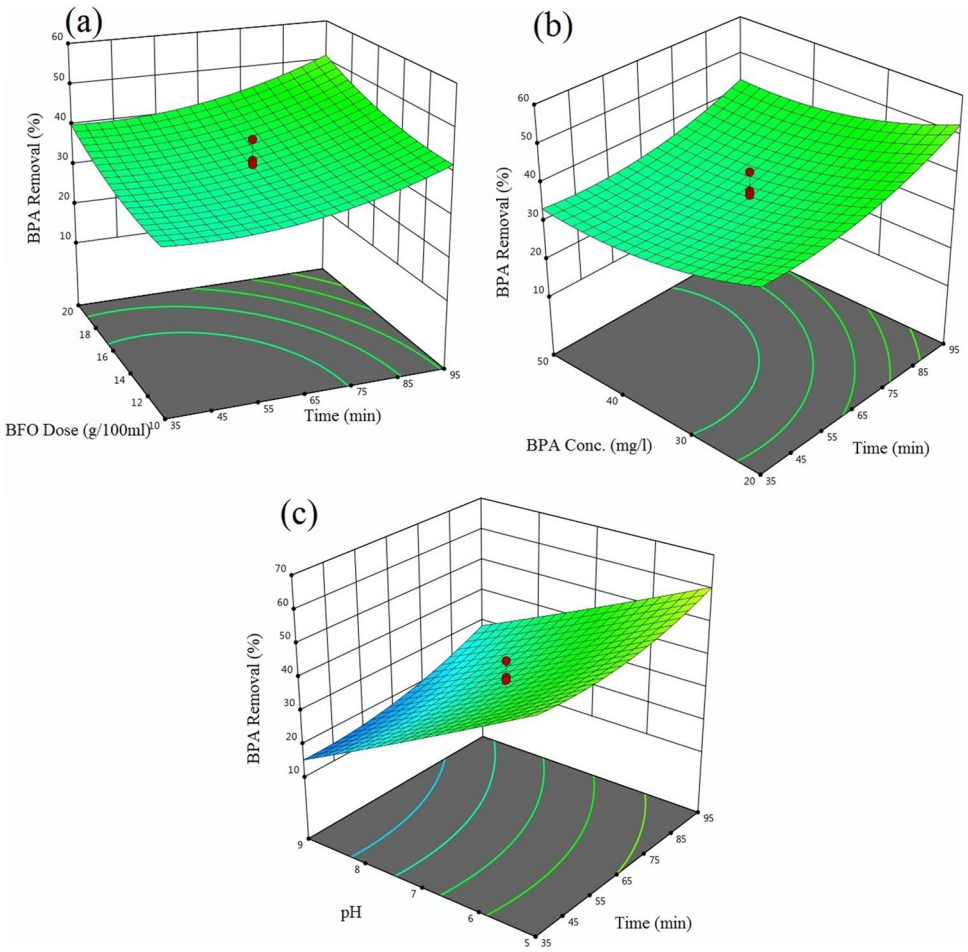

Fig. 3 3D surface plots of interaction effect of variables on BPA removal efficiency (%) as a function of **a** photocatalytic dosage and contact time, **b** initial BPA concentration and time; **c** pH and contact time

Kinetic studies

Figure 4 shows the dynamic model of BPA degradation by BFO NMPs. As mentioned earlier, the calculation of kinetics experiment in photocatalytic-oxidation process was performed in optimal condition. The correlation coefficients (R^2) of different kinetic including zero order, first order and second order are presented in Fig.4a–c. The results showed that the BPA degradation correlation coefficient is fitted to first-order model better than other one with $R^2 > 0.984$ ($y = -0.0281x + 2.3939$). This suggests that 1st model best defines the experimental data from BPA degradation, hence

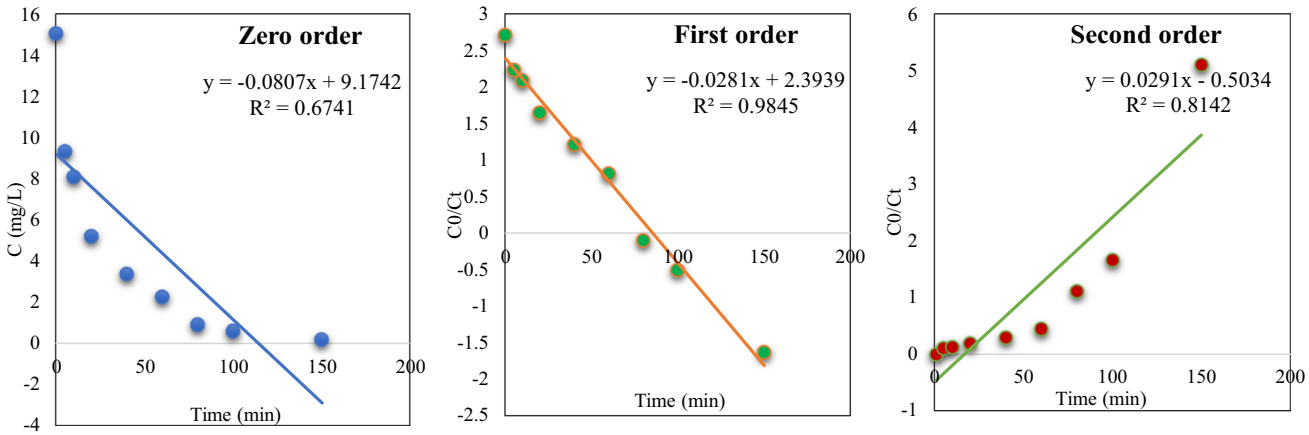

Fig. 4 Compatibility between different kinetic models with experimental data from BPA degradation by BFO NMPs under optimized conditions

recommending the high capability of model to fit the data gained from BPA degradation in the photocatalytic process.

Mineralization and reusability

TOC analyses were performed to determine the mineralization degree of BPA by BFO NMPs under optimized conditions (Fig. 5a). BPA degradation efficiency was found to be 98.7%, but the amount of TOC decreased by 87% after reaction. This phenomenon can be ascribed to the fact that the consumption of free radicals by BPA and other products resulting from degradation led to the removal of TOC less than the degradation efficiency (%) of BPA under the same experimental conditions.

The visible light photocatalytic stability of the BFO NMPs was investigated by recycling photodegradation experiments under optimized conditions for 5 cycles. After every cycle, the photocatalyst was separated by external magnet, then dried at 60 °C for 10 h and then reused in the next cycle. The degradation efficiencies of BFA for different cycles after visible light irradiation is displayed in Fig.5b. the Figure shows that the photodegradation efficiency decreases slightly with the increment of cycles and is still over 82% of that for the first cycling run at the fifth cycle, indicating that the visible light photocatalytic stability of the investigated nanocomposites is well. Meanwhile, a small amount of bismuth and iron leaching from BFO was observed (ranging from 0.01 to 0.005 mg/L for Bi and 0.158 to 0.11 mg/L for Fe) during 5 reuse cycles, suggesting good stability of catalyst (Fig. 5c). The high stability of the nanoparticles can be attributed to its metal- oxide structure.

Comparison with previous studies

The efficacy of the proposed systems in terms of BPA degradation efficiency was compared with the obtained results from previous studies over the last decade. Table 4 presents a summary of the findings. It can be clearly found that the BFO + UV system has a higher degradation capacity than the other methods. On the other hand, the optimum dose and time have a lower value than the majority of studies conducted so far. Based on the evidence, it can be reported

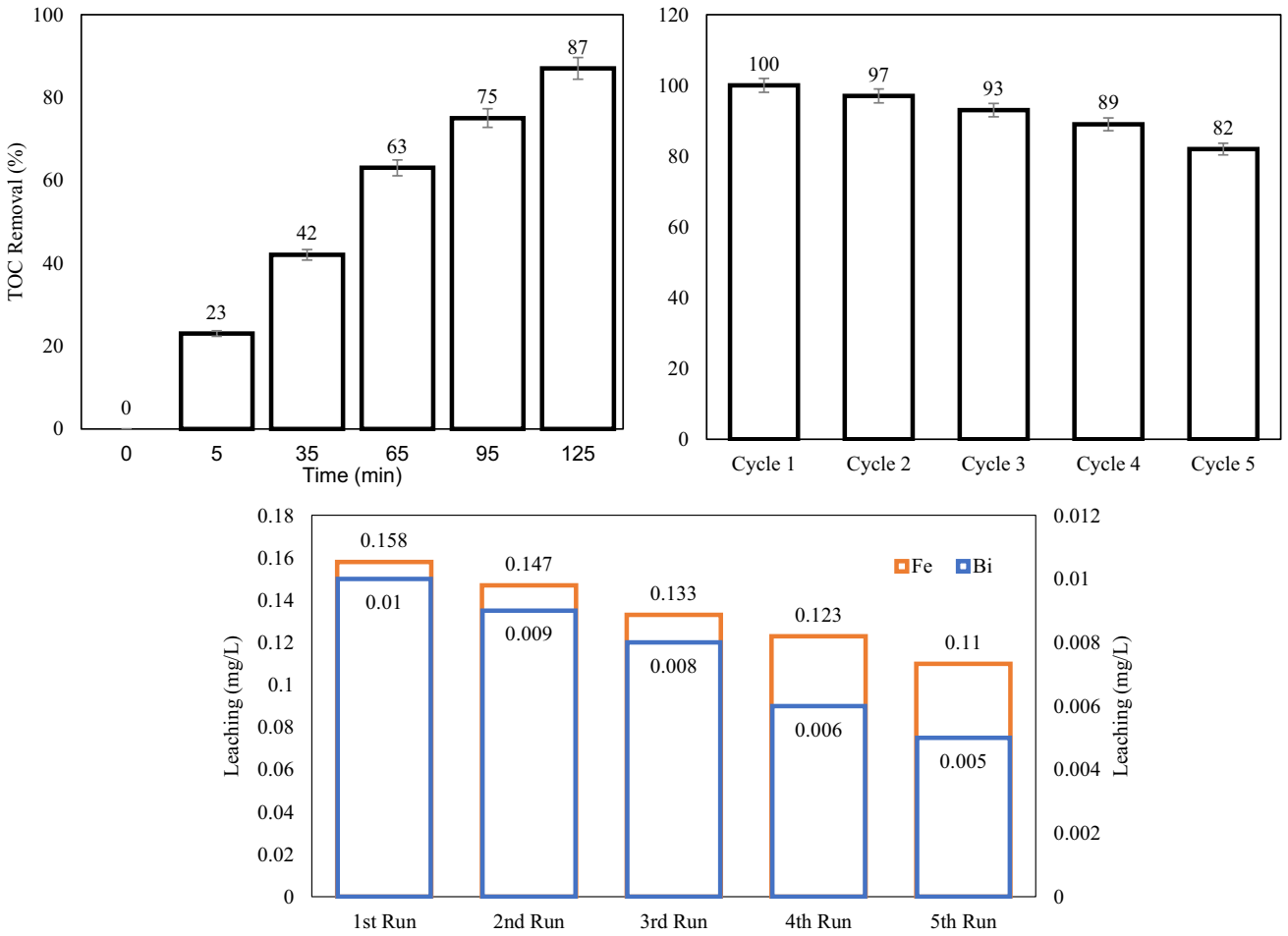

Fig. 5 The changes of TOC (a) and recycling tests (b) of BFO NMPs under optimized conditions for 5 cycles

Table 4 Comparison of BPA degradation in photocatalytic process under visible light irradiation reported in the literature

Catalysts	pollutant	BPA concentration mg/l	Time (min)	Dose (g/L)	pH (−)	Degradation (%)	References
TiO_2	BPA	25	120	0.1	3	100	[55]
TiO_2–3@ND	BPA	10	100	0.08	2.5	93	[56]
BFO	BPA	50	170	0.5	5.5	80	[34]
BFOPMS	BPA	50	130	0.45	2.5	100	[57]
BFO-MnO_2	BPA	20	130	0.3	5	63	[58]
Bi_2WO_6/BiOI@Ag_3PO_4	BPA	25	120	1	3	71	[59]
GO@BiOI/Bi_2WO_6	BPA	10	300	0.5	3	82	[60]
PLYS-Fe_3O4@TiO_2	BPA	25	120	1.5	3	100	[61]
TiO_2	BPA	20	140	0.07	3	95	[62]

that BFO MNPs with radiation visible light system has a good ability to remove BPA and can be used promisingly in the treatment (oxidation) of pollutants.

Degradation mechanism

Based on studies by Jiao [63], Nguyen [64] and Zhu [65] et al., the degradation intermediates were identified by GC-MS analysis and five main aromatic intermediates were determined including 2,2-bis(4-hydroxyphenyl)-1-propanol (m/z 230), 4-hydroxybenzoate (m/z 138), 4-hydroxyacetophenone (m/z 136), formic acid (m/z 46) and acetic acid (m/z 60). The BPA photocatalytic degradation mechanism can be supposed as follows; firstly, both photogenerated holes and hydroxyl radicals attack quaternary carbon atoms in BPA, resulting in the formation 2,2-bis(4- hydroxyphenyl)-1-propanol. Secondly, the covalent band between C–C bond of 2,2-bis(4-hydroxyphenyl)-1-propanol maybe attacked by hydroxyl radicals or via C-C scission reaction, which leads to the production of 4-hydroxyacetophenone and 4-hydroxybenzoate. Moreover, these intermediates compound could be oxidized to acetic acids and formic acids. Ultimately, the aromatic intermediates were degraded into ring-opening (branch chain) compounds and then sebsequently mineralized into H_2O and CO_2, resulting in the reduction of TOC concentration. Based on the identified intermediate products, a possible degradation pathway of BPA by BFO MNPs under visible light was proposed primarily (Fig. 6).

Conclusions

In the present study, BFO MNPs was synthesized and was successfully developed for BPA treatment from queues solution. A multi-response optimization based on CCD approach was applied to predict and optimize the effect of pH, contact time, catalyst dosage and BPA concentration on BPA removal. The results of ANOVA test revealed that the effect of main parameters on the performance of the BPA removal was significant with Prob > F < = 0.05. The Fmodel = 40.87 and P-values = 0.0001 show that model terms have significant effect on degradation process. The higher predicted degradation efficiency (100%) is obtained at pH = 4.042, catalyst dose = 7.617 mg, contact time = 122.742 min and BPA concentration = 15.065 mg/L. Reusability of BFO NMPs for 5 successive cycles showed a decrease in efficiency about 18%. As a result, the findings in this paper indicated that BFO MNPs visible light iradation could be used as an efficient method for decreasing BPA compound from aqueous solution.

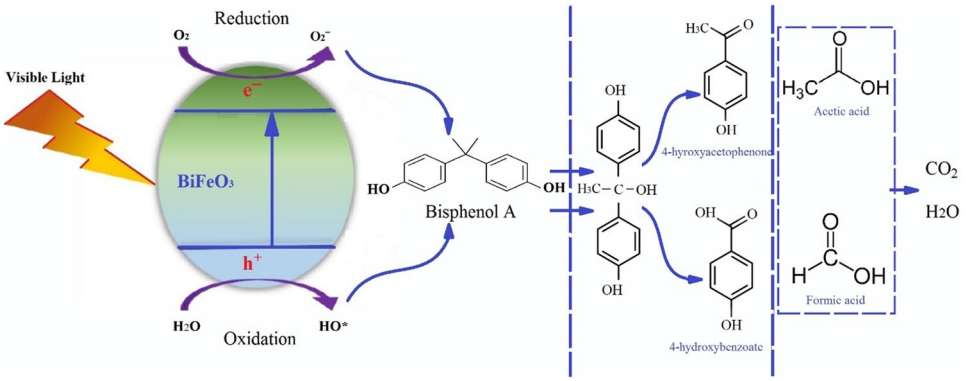

Fig. 6 Proposed photodegradation mechanism and pathway of BPA over BFO MNPs under visible light irradiation

Acknowledgements This study was funded by Tehran University of Medical Sciences (TUMS), Institute for Environmental Research with research code of 96-03-46-36266. Hence, the authors would like to express their gratitude for this support.

Declarations

Conflict of interest All authors certify that they have no affiliations with or involvement in any organization or entity with any financial interest or non-financial interest in the subject matter or materials discussed in this manuscript.

References

1. Mahvi AH, et al. Photo-oxidation of phenol in aqueous solution: toxicity of intermediates. Korean J Chem Eng. 2007;24(1):79–82.
2. Bazrafshan E, Biglari H, Mahvi AH. Phenol removal by electrocoagulation process from aqueous solutions. Fresenius Environ Bull. 2012;21(2):364–71.
3. Biglari H, et al. A review and investigation of the effect of nano-photocatalytic ozonation process for phenolic compound removal from real effluent of pulp and paper industry. Environ Sci Pollut Res. 2017;24(4):4105–16.
4. Maleki A, et al. Degradation and toxicity reduction of phenol by ultrasound waves. Bull Chem Soc Ethiop. 2007;21(1).
5. Bazrafshan E, Mostafapour FK, Mahvi AH. Phenol removal from aqueous solutions using pistachio-nut shell ash as a low cost adsorbent. Fresenius Environ Bull. 2012;21(10):2962–8.
6. Davididou K, et al. Photocatalytic degradation of bisphenol-a under UV-LED, blacklight and solar irradiation. J Clean Prod. 2018;203:13–21.
7. Nikfar E, et al. Removal of bisphenol a from aqueous solutions using ultrasonic waves and hydrogen peroxide. J Mol Liq. 2016;213:332–8.
8. Liao C, Kannan K. Concentrations and profiles of bisphenol a and other bisphenol analogues in foodstuffs from the United States and their implications for human exposure. J Agric Food Chem. 2013;61(19):4655–62.
9. Abo R, Kummer N-A, Merkel BJ. Optimized photodegradation of bisphenol a in water using ZnO, TiO 2 and SnO 2 photocatalysts under UV radiation as a decontamination procedure. Drinking Water Engineering and Science. 2016;9(2):27–35.
10. Calafat AM, et al. Exposure of the US population to bisphenol a and 4-tertiary-octylphenol: 2003–2004. Environ Health Perspect. 2008;116(1):39–44.
11. Pelch K, et al. A scoping review of the health and toxicological activity of bisphenol a (BPA) structural analogues and functional alternatives. Toxicology. 2019;424:152235.
12. Dehghani MH, et al. Adsorption of bisphenol a (BPA) from aqueous solutions by carbon nanotubes: kinetic and equilibrium studies. Desalin Water Treat. 2015;54(1):84–92.
13. Bechambi O, Sayadi S, Najjar W. Photocatalytic degradation of bisphenol a in the presence of C-doped ZnO: effect of operational parameters and photodegradation mechanism. J Ind Eng Chem. 2015;32:201–10.
14. Reddy PVL, et al. Photocatalytic degradation of bisphenol a in aqueous media: a review. J Environ Manag. 2018;213:189–205.
15. Abraham A, Chakraborty P. A review on sources and health impacts of bisphenol a. Rev Environ Health. 2020;35(2):201–10.
16. Gao B, et al. Zr-doped TiO2 for enhanced photocatalytic degradation of bisphenol a. Appl Catal A Gen. 2010;375(1):107–15.
17. Wang, X. and T.-T. Lim, *Solvothermal synthesis of C–N codoped TiO2 and photocatalytic evaluation for bisphenol A degradation using a visible-light irradiated LED photoreactor.* Appl Catal B Environ, 2010. 100(1): p. 355–364.
18. Asadgol Z, et al. Removal of phenol and bisphenol-a catalyzed by laccase in aqueous solution. J Environ Health Sci Eng. 2014;12(1):1–5.
19. Chen J, Huang X, Lee D. Bisphenol a removal by a membrane bioreactor. Process Biochem. 2008;43(4):451–6.
20. Dong Y, et al. Adsorption of bisphenol a from water by surfactant-modified zeolite. J Colloid Interface Sci. 2010;348(2):585–90.
21. Mita L, et al. Bisphenol a removal by a Pseudomonas aeruginosa immobilized on granular activated carbon and operating in a fluidized bed reactor. J Hazard Mater. 2015;291:129–35.
22. Deborde M, et al. Oxidation of bisphenol a by ozone in aqueous solution. Water Res. 2008;42(16):4299–308.
23. Dehghan A, et al. Adsorption and visible-light photocatalytic degradation of tetracycline hydrochloride from aqueous solutions using 3D hierarchical mesoporous BiOI: synthesis and characterization, process optimization, adsorption and degradation modeling. Chem Eng Res Des. 2018;129:217–30.
24. Dong W, et al. Excellent photocatalytic degradation activities of ordered mesoporous anatase TiO2–SiO2 nanocomposites to various organic contaminants. J Hazard Mater. 2012;229-230:307–20.
25. Saravanan R, et al. Enhanced photocatalytic activity of ZnO/CuO nanocomposite for the degradation of textile dye on visible light illumination. Mater Sci Eng C. 2013;33(1):91–8.
26. Gupta VK, et al. Removal of the hazardous dye—Tartrazine by photodegradation on titanium dioxide surface. Mater Sci Eng C. 2011;31(5):1062–7.
27. Pattnaik SP, et al. Synthesis, photoelectrochemical properties and solar light-induced photocatalytic activity of bismuth ferrite nanoparticles. J Nanopart Res. 2018;20(1):10.
28. Soltani T, Entezari MH. Solar photocatalytic degradation of RB5 by ferrite bismuth nanoparticles synthesized via ultrasound. Ultrason Sonochem. 2013;20(5):1245–53.
29. Lu H, et al. Enhanced photocatalytic performance of ag-decorated BiFeO3 in visible light region. J Sol-Gel Sci Technol. 2015;76(1):50–7.
30. Ponraj C, V G, Daniel J. A review on the visible light active BiFeO3 nanostructures as suitable photocatalyst in the degradation of different textile dyes. Environmental Nanotechnology, Monitoring & Management. 2017;7:110–20.
31. Dehghani MH, et al. Removal of methylene blue dye from aqueous solutions by a new chitosan/zeolite composite from shrimp waste: kinetic and equilibrium study. Korean J Chem Eng. 2017;34(6):1699–707.
32. Dehghani MH, Dehghan A, Najafpoor A. Removing reactive red 120 and 196 using chitosan/zeolite composite from aqueous solutions: kinetics, isotherms, and process optimization. J Ind Eng Chem. 2017;51:185–95.
33. Karami A, et al. Application of response surface methodology for statistical analysis, modeling, and optimization of malachite green removal from aqueous solutions by manganese-modified pumice adsorbent. Desalin Water Treat. 2017;89:150–61.
34. Soltani T, Lee B-K. Sono-synthesis of nanocrystallized BiFeO3/reduced graphene oxide composites for visible photocatalytic degradation improvement of bisphenol a. Chem Eng J. 2016;306:204–13.
35. Liu Y, et al. A novel synergy of Er3+/Fe3+ co-doped porous Bi5O7I microspheres with enhanced photocatalytic activity under visible-light irradiation. Appl Catal B Environ. 2017;205:421–32.
36. Mohapatra DP, et al. Parameter optimization of ferro-sonication pre-treatment process for degradation of bisphenol a and biodegradation from wastewater sludge using response surface model. J Hazard Mater. 2011;189(1):100–7.
37. Khataee AR, et al. Optimization of photocatalytic treatment of dye solution on supported TiO2 nanoparticles by central

composite design: intermediates identification. J Hazard Mater. 2010;181(1):886–97.
38. Mosleh S, et al. Photocatalytic degradation of binary mixture of toxic dyes by HKUST-1 MOF and HKUST-1-SBA-15 in a rotating packed bed reactor under blue LED illumination: central composite design optimization. RSC Adv. 2016;6(21):17204–14.
39. Vaez M, Zarringhalam Moghaddam A, Alijani S. Optimization and modeling of photocatalytic degradation of azo dye using a response surface methodology (RSM) based on the central composite design with immobilized Titania nanoparticles. Ind Eng Chem Res. 2012;51(11):4199–207.
40. Soleymani AR, et al. Modeling and optimization of a sono-assisted photocatalytic water treatment process via central composite design methodology. Process Saf Environ Prot. 2015;94:307–14.
41. Amalraj Appavoo I, et al. Response surface modeling of carbamazepine (CBZ) removal by graphene-P25 nanocomposites/UVA process using central composite design. Water Res. 2014;57:270–9.
42. Liu H-L, Chiou Y-R. Optimal decolorization efficiency of reactive red 239 by UV/TiO2 photocatalytic process coupled with response surface methodology. Chem Eng J. 2005;112(1):173–9.
43. Xue Z, et al. Degradation of tetracycline with $BiFeO_3$ prepared by a simple hydrothermal method. Materials (Basel, Switzerland). 2015;8(9):6360–78.
44. Gao F, et al. Visible-light photocatalytic properties of weak magnetic BiFeO3 nanoparticles. Adv Mater. 2007;19(19):2889–92.
45. Soltani T, Entezari MH. Photolysis and photocatalysis of methylene blue by ferrite bismuth nanoparticles under sunlight irradiation. J Mol Catal A Chem. 2013;377:197–203.
46. Gao T, et al. Synthesis of BiFeO3 nanoparticles for the visible-light induced photocatalytic property. Mater Res Bull. 2014;59:6–12.
47. Senthilnathan J, Philip L. Photocatalytic degradation of lindane under UV and visible light using N-doped TiO2. Chem Eng J. 2010;161(1):83–92.
48. Hao C, et al. Photocatalytic performances of BiFeO3 particles with the average size in nanometer, submicrometer, and micrometer. Mater Res Bull. 2014;50:369–73.
49. Huo Y, Jin Y, Zhang Y. Citric acid assisted solvothermal synthesis of BiFeO3 microspheres with high visible-light photocatalytic activity. J Mol Catal A Chem. 2010;331(1–2):15–20.
50. Seck EI, et al. Photocatalytic removal of 2,4-dichlorophenoxyacetic acid by using sol–gel synthesized nanocrystalline and commercial TiO2: operational parameters optimization and toxicity studies. Appl Catal B Environ. 2012;125:28–34.
51. Khataee AR, Kasiri MB, Alidokht L. Application of response surface methodology in the optimization of photocatalytic removal of environmental pollutants using nanocatalysts. Environ Technol. 2011;32(15):1669–84.
52. Zhu H, et al. Effective photocatalytic decolorization of methyl orange utilizing TiO2/ZnO/chitosan nanocomposite films under simulated solar irradiation. Desalination. 2012;286:41–8.
53. Cao C, et al. Visible-light photocatalytic decolorization of reactive brilliant red X-3B on Cu2O/crosslinked-chitosan nanocomposites prepared via one step process. Appl Surf Sci. 2013;271:105–12.
54. Wang H, et al. Preparing a photocatalytic Fe doped TiO2/rGO for enhanced bisphenol a and its analogues degradation in water sample. Appl Surf Sci. 2020;505:144640.
55. Chiang K, et al. Photocatalytic degradation and mineralization of bisphenol a by TiO2 and platinized TiO2. Appl Catal A Gen. 2004;261(2):225–37.
56. Hunge Y, et al. Photocatalytic degradation of bisphenol a using titanium dioxide@ nanodiamond composites under UV light illumination. J Colloid Interface Sci. 2021;582:1058–66.
57. Soltani T, Tayyebi A, Lee B-K. Quick and enhanced degradation of bisphenol a by activation of potassium peroxymonosulfate to SO4− with Mn-doped BiFeO3 nanoparticles as a heterogeneous Fenton-like catalyst. Appl Surf Sci. 2018;441:853–61.
58. Li L, et al. Enhanced mineralization of bisphenol a by eco-friendly BiFeO3–MnO2 composite: performance, mechanism and toxicity assessment. J Hazard Mater. 2020;399:122883.
59. Chu Y, et al. Fabrication of flower-globular Bi2WO6/BiOI@ Ag3PO4 photocatalyst for the degradation of bisphenol a and cefepime under sunlight: photoelectric properties, degradation performance, mechanism and biodegradability enhancement. Sep Purif Technol. 2021;272:118866.
60. Mengting Z, et al. 2D graphene oxide (GO) doped pn type BiOI/Bi2WO6 as a novel composite for photodegradation of bisphenol a (BPA) in aqueous solutions under UV-vis irradiation. Mater Sci Eng C. 2020;108:110420.
61. Li X, et al. Application of pea-like yolk–shell structured Fe 3 O 4@ TiO 2 nanosheets for photocatalytic and photo-Fenton oxidation of bisphenol-a. RSC Adv. 2019;9(38):22153–60.
62. Garg A, et al. Photocatalytic degradation of bisphenol-a using N, co Codoped TiO 2 catalyst under solar light. Sci Rep. 2019;9(1):1–13.
63. Jiao Z, et al. Degradation of bisphenol a by CeCu oxide catalyst in catalytic wet peroxide oxidation: efficiency, stability, and mechanism. Int J Environ Res Public Health. 2019;16(23):4675.
64. Nguyen, T.B., C. Huang, and R.-a. Doong, Photocatalytic degradation of bisphenol a over a ZnFe2O4/TiO2 nanocomposite under visible light. Sci Total Environ, 2019. 646: p. 745–756.
65. Zhu Y, et al. Efficient activation of persulfate by Fe 3 O 4@ β-cyclodextrin nanocomposite for removal of bisphenol a. RSC Adv. 2018;8(27):14879–87.